(NASA-CR-169278) TURBINE ENDWALL SINGLE CYLINDER PROGRAM Semiannual Status Report, 1 Jan. - 1 Jul. 1982 (Connecticut Univ.) 50 p HC A03/MF A01 CSCL 20D

N82-31638

Unclas
G3/34 28770

MECHANICAL ENGINEERING DEPARTMENT

SCHOOL OF ENGINEERING
THE UNIVERSITY OF CONNECTICUT
STORRS, CONNECTICUT

TURBINE ENDWALL SINGLE CYLINDER PROGRAM

Semi-Annual Status Report

Grant No. NSG 3238

January 1, 1982 - July 1, 1982

Submitted to:

Lewis Research Center

National Aeronautics and Space Administration
21000 Brookpark Road
Cleveland, Ohio 44135

Principal Investigator:

Lee S. Langston
Associate Professor
Department of Mechanical Engineering
University of Connecticut
Storrs, Connecticut 06268

Introduction

The following is a report of progress made during the first six months (January 1, 1982 to July 1, 1982) under the second phase of NASA Grant No. NSG 3238. (Work is underway to complete the final reports on the first phase of this grant)

Under this second phase, detailed measurement will be taken of the flow field in front of a large-scale single cylinder, mounted in a wind tunnel. These measurements will provide a better understanding of the three-dimensional separation occuring in front of the cylinder on the endwall, and of the vortex system that is formed. The measurements will also provide a data base with which to check analytical and numerical computer models of three-dimensional flows.

The work that will be reported on is as follows:

a) A literature survey of three-dimensional boundary layers and their separation, single cylinder experiments, and a brief survey of fluid flow calculation methods.

b) Modifications to the wind tunnel, and the design and fabrication of the model.

c) Five-hole probe calibrations.

d) Description of the data acquisition system.

e) Asymmetric model of saddle point flow.

Literature Survey

The flow separation caused by an adverse pressure gradient generated from a bluff body is a three-dimensional problem. To describe this three-dimensionality, consider a viscous flow over an infinite flat plate. The velocity

vectors in the boundary layer vary in magnitude normal to the plate, from zero at the plate surface to the free-stream value at the edge of the boundary layer. In addition, the velocity magnitude may vary in the flow direction if a pressure gradient exists, such as the adverse pressure gradient imposed by a two-dimensional step. Since the pressure gradient imposed by such a step is uniform in the transverse direction, the mean velocity vectors do not have a transverse component so that the flow is two-dimensional even through the separation in front of the step. Now consider the case where the boundary layer approaches a bluff body, such as a cylinder, instead of a two-dimensional step. In this case, the adverse pressure gradient imposed on the flow varies in the transverse direction inducing transverse velocity components. The separation that develops in front of the bluff body, then, is three-dimensional. For the range of Reynolds number of interest in this program, the boundary layer is turbulent. Therefore, a literature survey has been conducted to identify investigations that have been accomplished on three-dimensional separating turbulent flows.

The study of three-dimensional turbulent boundary layers has been approached analytically in three areas. One of the approaches has been to apply kinematical principles and theorems to the fluid flow in order to qualitatively infer the flow processes in the separation region. A second approach has been to use integral methods to solve the three-dimensional momentum integral equations. The third technique involves solving the differential boundary layer equations using numerical approximations. A discussion of the results of these approaches follows.

Before presenting details of the above approaches, a summary of the terminology associated with three-dimensional boundary layers, based on Nash and Patel[1], is given. The mean velocity profile in a three-dimensional

boundary layer is composed of the velocity vectors along a normal to the body surface. Since the velocity profile is generally not collateral (the velocity vectors do not lie in a plane as for a two-dimensional boundary layer), its graphical depiction is more difficult than a two-dimensional profile. An isometric representation of the velocity profile in a three-dimensional boundary layer is shown in Fig.1. This type of boundary layer, in which the velocity varies in both magnitude and direction is referred to in the literature as a skewed boundary layer. The isometric representation conveys the profile's general form but is not ideal for quantitative examination. Two-dimensional representations of the profile are often more useful for evaluating the flow. They usually take the form either of projections of the profile onto suitably oriented planes, or of separate plots of the magnitude and direction of the magnitude and direction of the velocity vectors.

Figure 2 shows the latter representation where the velocity magnitude, u, normalized by the resultant velocity at edge of the boundary layer, $u_{s_{ms}}$, and the angle ε which the velocity vector makes with some datum, are plotted as a function of y, the normal distance from the body surface. In this example, ε was chosen to be the angle measured relative to the streamline at the outer edge of the boundary layer. This angle is usually referred to as the crossflow angle, with the crossflow angle at y=0 being the wall crossflow angle, ε_w. Alternatively, the velocity profile can be represented by its projection on any two nonparallel planes. Orthogonal planes are usually chosen for convenience. The dashed curves in Fig.1 show the projections onto two orthogonal planes whose line of intersection is the normal to the body surface at the point at which the profile is measured. In Fig.1, the angular orientation of the orthogonal planes has no special significance. Often times the orthogonal planes are oriented so

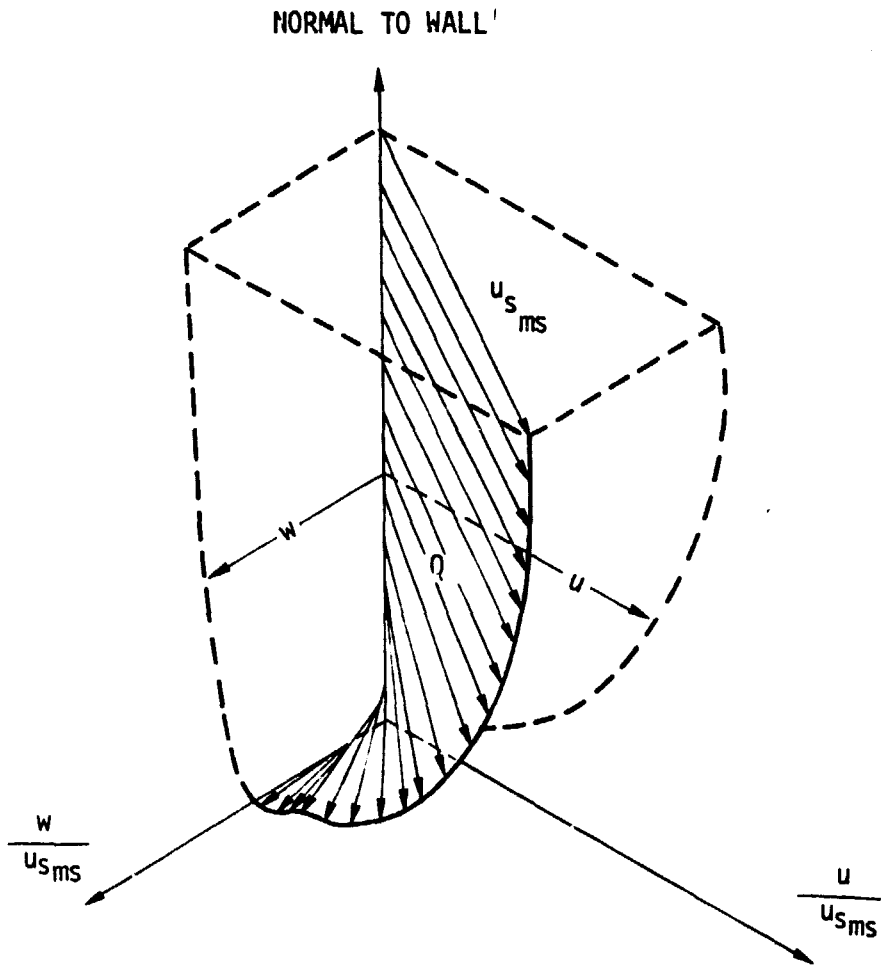

Figure 1. Isometric view of a three-dimensional mean velocity profile

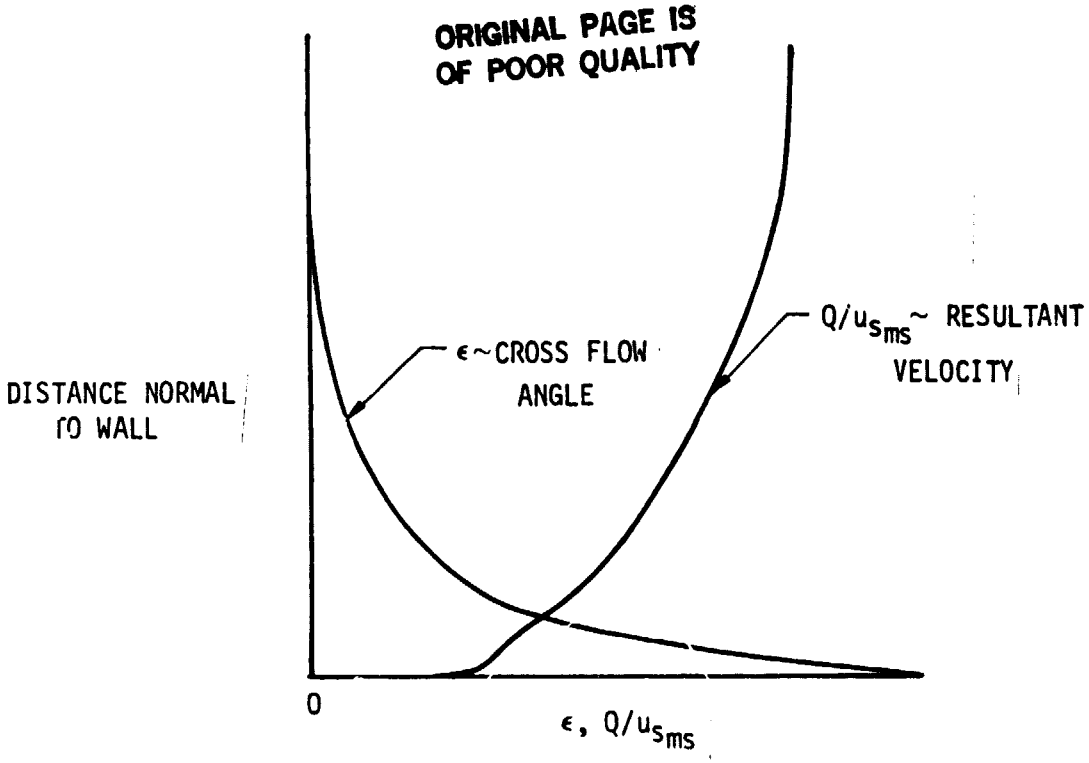

Figure 2. Profile of velocity magnitude and direction

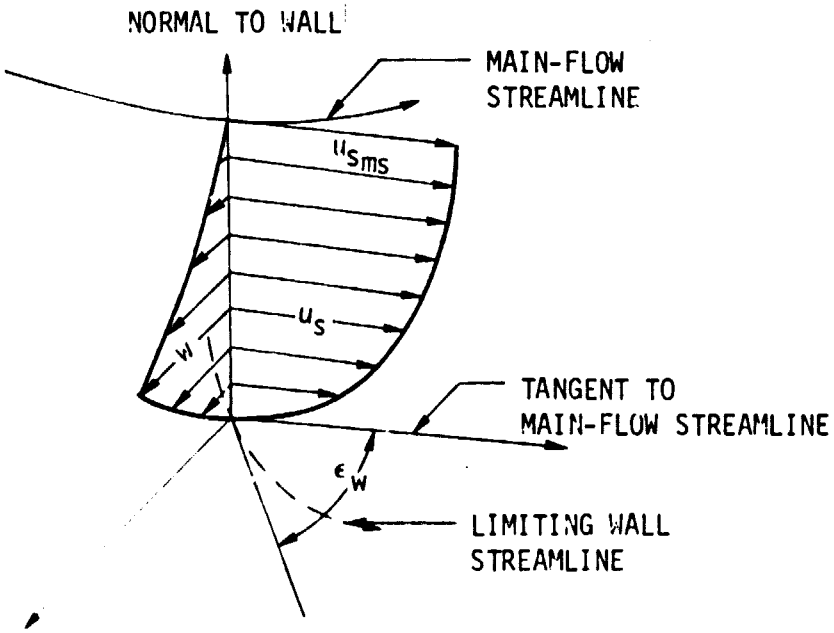

Figure 3. Streamline coordinate system

that one of the planes is parallel to the streamlines at the outer edge of the boundary layer. This coordinate system, referred to as streamline coordinates and shown in Fig.3, produces a pair of unique curves for u_s and u_n, Fig.4, where the streamwise velocity component $u_s(y)$ is measured parallel to the external streamlines and the crossflow or secondary-flow component $u_n(y)$ is measured normal to the external streamline. u_n naturally falls to zero at the edge of the boundary layer.

Another type of two-dimensional projection is the polar plot shown in Fig.5. In this case using streamline coordinates, the velocity vectors are projected onto the plane tangential to the surface of the body, producing a plot of u_n vs. u_s. A straight line joining the origin to any point on the curve gives the magnitude and direction of the local velocity vector.

Separation is the generic name given to a class of flow phenomena. One feature which characterizes this class is that the flow becomes detached from the body surface allowing a turbulent region of indefinite extent to develop between the body and the outer, quasi-inviscid flow. Separation provides a mechanism whereby vorticity, which in attached flow is confined within the boundary layer, can be transported into the interior of the fluid. Prediction of the onset of separation is of considerable practical importance. In steady, incompressible, two-dimensional flow, the point of separation correlates with the point at which the skin friction falls to zero. This fortunate correlation has led to the adoption of zero wall shear stress as a separation criterion which is both precise and unambiguous. In three-dimensional flows, separation is rarely associated with the vanishing of the wall shear stress. In addition, separation is sometimes not associated with any special character of the flow at the surface. However, discussions of three-dimensional separation in the

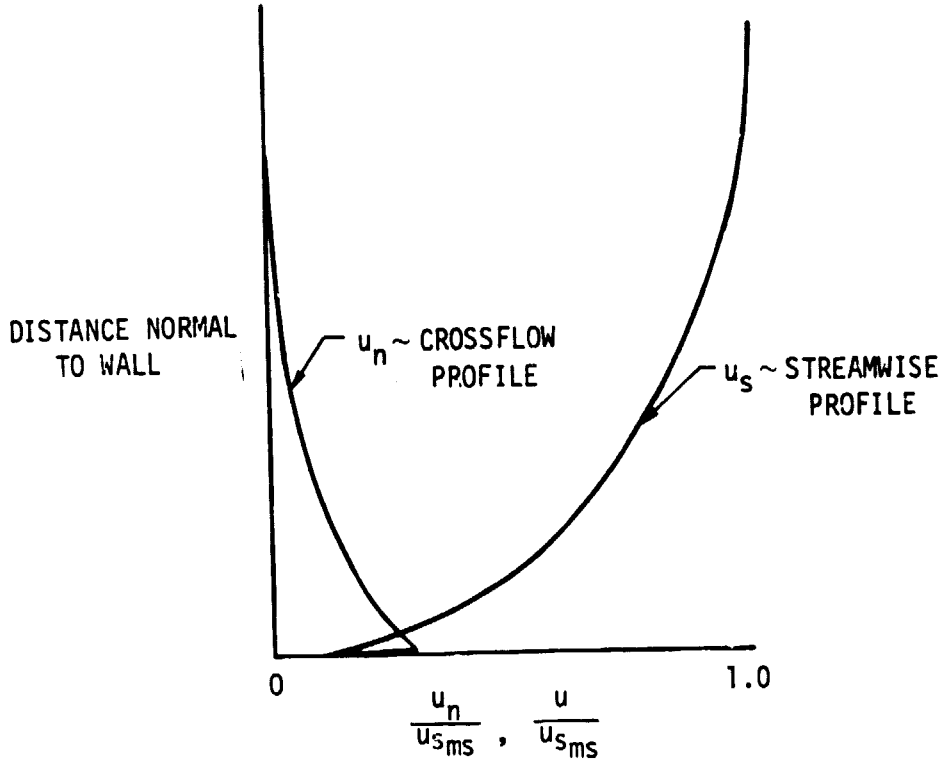

Figure 4. Velocity profile projected in streamwise and crossflow components

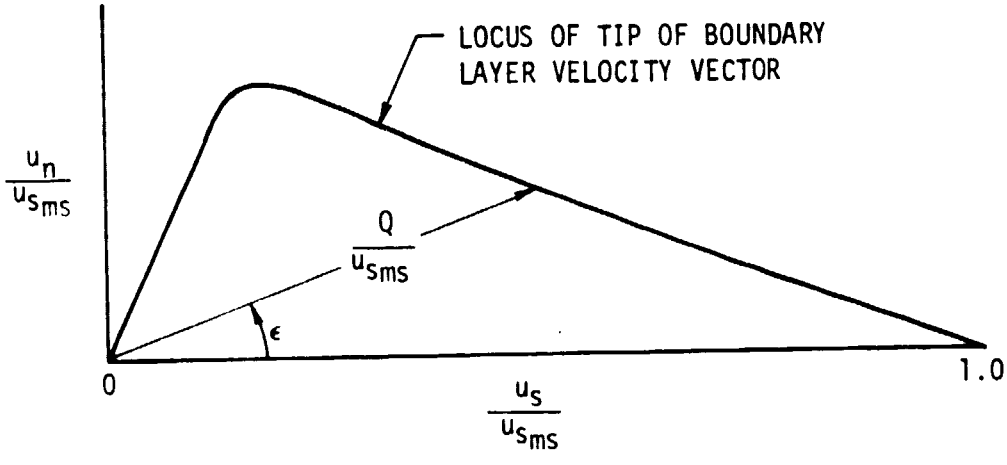

Figure 5. Polar plot of the mean velocity profile

literature have concentrated on the definition of separation in terms of surface-flow conditions and have attempted to find a rational extension of the zero-skin-friction criterion.

Maskell[2] presented the first generalized kinematical concept of separation in three dimensions. He defined limiting streamlines which represent the motion of fluid particles that pass infinitely close to a solid surface. The direction of these limiting streamlines, which are single-valued and tangent to the solid surface at all locations except at singular points defined below, is parallel to the wall shear-stress vector and can be inferred from surface flow visualization. Maskell defined a separation point to exist when two limiting streamlines combine at a point to form a separation streamline. If the limiting streamlines remain tangent to the solid surface, their direction is single-valued and continuous. Maskell defined this type of separation point as an ordinary point. However, if the combined limiting streamlines do not remain tangent to the solid surface, the wall shear stress vanishes and the limiting flow direction is discontinuous and many-valued. This separation point was termed a singular point. A separation zone then is bounded by a separation line made up of singular and ordinary points in Maskell's terminology. Maskell went on to characterize separation regions as consisting of free-vortex layers and bubbles, and he indicated the surface flow patterns associated with these two elements.

Limiting streamlines can be very useful because they can be used to quantitatively define the structure of the viscous region of the flow. In high Reynolds Number flows, the viscous region is well-defined so that knowledge of the forms that this structure might take is important to a proper understanding of the physical nature of any three-dimensional flow. However, as

indicated by Taylor[3], Maskell's approach has two drawbacks. The limiting streamlines are not ordinary streamlines since, in the limit, they lie on the solid surface. They approximate streamlines next to the solid surface, but when the boundary-layer thickness is changing rapidly, such as near a separation point, the limiting streamlines may not be indicative of ordinary streamlines. In addition, determination of whether the limiting streamlines are merely converging or actually combining to form separation streamlines can be very difficult for some flow patterns. Thus, interpretation of surface flow visualization for complex flow patterns must be accomplished very carefully.

In order to circumvent the above problems, Lighthill[4] introduced the concept of vorticity at the surface, which is equal to vorticity in the fluid. In addition, Lighthill proposed to identify separations by studying the topology of the entire surface rather than determining separation at a single point as proposed by Maskell. Lighthill classified the critical points based on derivitives of the shear-stress vector. In particular, critical points fell into two topological categories, depending on the value of the Jacobian, J, of the shear-stress vector:

(i) $J<0$: Saddle points, through which pass two shear-stress lines on each of which the direction of the shear stress changes when passing through the critical point.

(ii) $J>0$: Nodal points, through which pass an infinite number of shear stress lines either all into the point or all out of the point.

Lighthill further classified the critical points according to values of the divergence, Δ, of the shear-stress vector. For Δ greater than or less than zero, the critical points were considered attachment points or separation points,

respectively. In addition, nodal points for which $J>\Delta^2/4$ were categorized as foci. A summary of these classifications, with corresponding flow patterns as developed by Hunt et.al.[10], is contained in Fig.6. Lighthill identified the separation line as the line joining a saddle point to a nodal point. However, as discussed by Taylor[3], Lighthill's separation criteria would be difficult to apply for situations where the singularities may be far upstream or downstream.

Oswatitsch[5] investigated the conditions for the separation of a three-dimensional boundary layer using the phase-plane technique developed in the field of dynamics. He assumed the velocity components were expandable into a Taylor series about the critical point. Using the Navier-Stokes equations, continuity equation, and the no-slip condition for a viscous fluid, he was able to parametrically determine the trajectory of the streamlines adjacent to a singular separation point. Oswatitsch showed the types of separation flow patterns that are predicted by his model for cases of both symmetrical and asymmetrical three-dimensional separations.

Based on the discussion of Taylor[3], Kronauer[6] indicated that the problem of finding a separation line is the same as finding the limit trajectories of the governing differential equation set. Perry and Fairlie[7] followed the suggestion of Kronauer and explored the properties of the governing partial differential equations using the phase-space method. The authors identified surface critical points and streamline patterns for both a viscous real fluid and an inviscid rotational flow. The latter case was considered to be the appropriate model for turbulent boundary layers approaching an obstacle based on previous work of Smith[8] on the flow in the region of an aero-foil trailing edge and Fairlie[9] relative to two-dimensional separation bubbles. In contrast to the case where viscosity is included, solving the inviscid equations in this manner indicates

SADDLE POINTS

$J < 0$

$\Delta < 0$

(SEPARATION POINT)

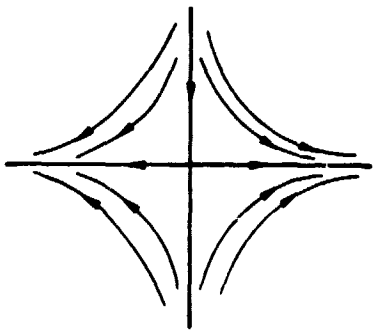

$\Delta > 0$

(ATTACHMENT POINT)

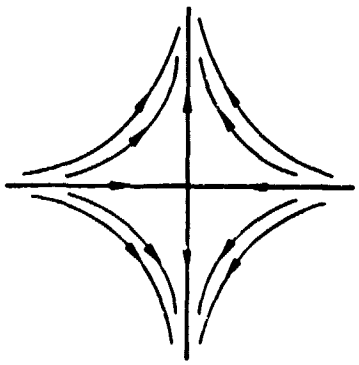

NODAL POINTS

$\frac{\Delta^2}{4} > J > 0$

$\Delta < 0$

(SEPARATION POINT)

$\Delta > 0$

(ATTACHMENT POINT)

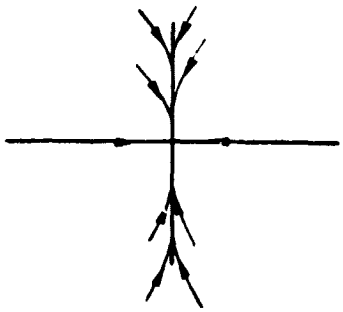

$J > \Delta^2/4$

(FOCI)

$\Delta < 0$

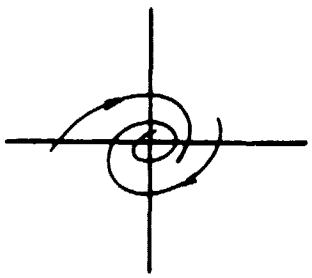

$\Delta > 0$

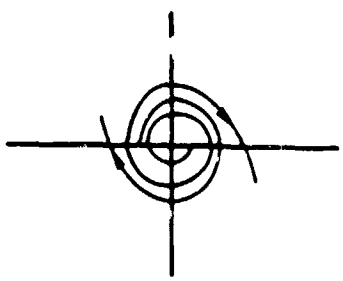

Figure 6. Singular point classification proposed by Lighthill

that all the pressure gradients vanish at the critical point. This is a significant difference from the analysis of Oswatitsch where the pressure gradients determine the type of flow. Thus, true surface patterns in turbulent flow can be predicted with this technique only by matching the inviscid patterns obtained by Perry and Fairlie to those produced in the viscous zone. Perry and Fairlie did not develop a relationship for the number of nodes and saddle points that can exist, though restrictions were developed for pressure and vorticity for various critical points.

Hunt, et.al.[10], using previous topological work on separated flow, developed rules for the number of nodes and saddle points that must be present for a postulated separation flow pattern to be kinematically possible. Extending the work of Lighthill[4] and Flegg[11], Hunt et.al. determined that, with a three-dimensional body on a plane, the total number of nodes must equal the total number of saddle points on the surface plane:

$$\Sigma_N - \Sigma_S = 0 \tag{1}$$

where Σ_N = total number of nodes

Σ_S = total number of saddle points

They also found that when considering the mean streamlines in a two-dimensional plane containing a singly connected region, as investigated by Perry and Fairlie, the following relationship holds:

$$(\Sigma_N + 1/2\ \Sigma_N') - (\Sigma_S + 1/2\ \Sigma_S') = 0 \tag{2}$$

where Σ_N' = total number of surface nodes

Σ_S' = total number of surface saddle points

Σ_N = total number of nodes excluding surface nodes

Σ_S = total number of saddle points excluding surface saddle points.

An illustration of the application of the equation 2 is given in Fig.7, which represents the postulated centerline flow pattern around the cube taken from Hunt, et.al. The above relationships can be effective tools for verifying that derived flow fields based on experimental data are consistent with kinematic principles.

Although the application of kinematic principles to three-dimensional boundary layer separations provides illustrative information regarding the flow processes, quantitative analytical information can only be obtained by solving the governing equations. One technique is to integrate the boundary layer equations to form two momentum-integral equations. These equations are coupled first-order differential equations involving eight dependent variables for an orthogonal coordinate system. By using a streamline coordinate system, the determination of which in general three-dimensional flows can be a formidable problem, the integral equations are considerably simpler, and one of the parameters can be eliminated. The problems facing users of the integral technique then, is to determine five auxiliary equations in order to close the solution. Formulation of these relationships has been accomplished by postulating the existence of a velocity-profile family both in the streamwise and crossflow directions. These velocity profiles must be universal in order to use integral techniques to predict general three-dimensional flows. However, no such universal profile has been developed, with efforts to formulate a universal crossflow profile the least fruitful. A summary of attempts to develop such a crossflow profile follows.

The earliest crossflow model is due to Prandtl[12], who suggested the following formulation for small crossflows:

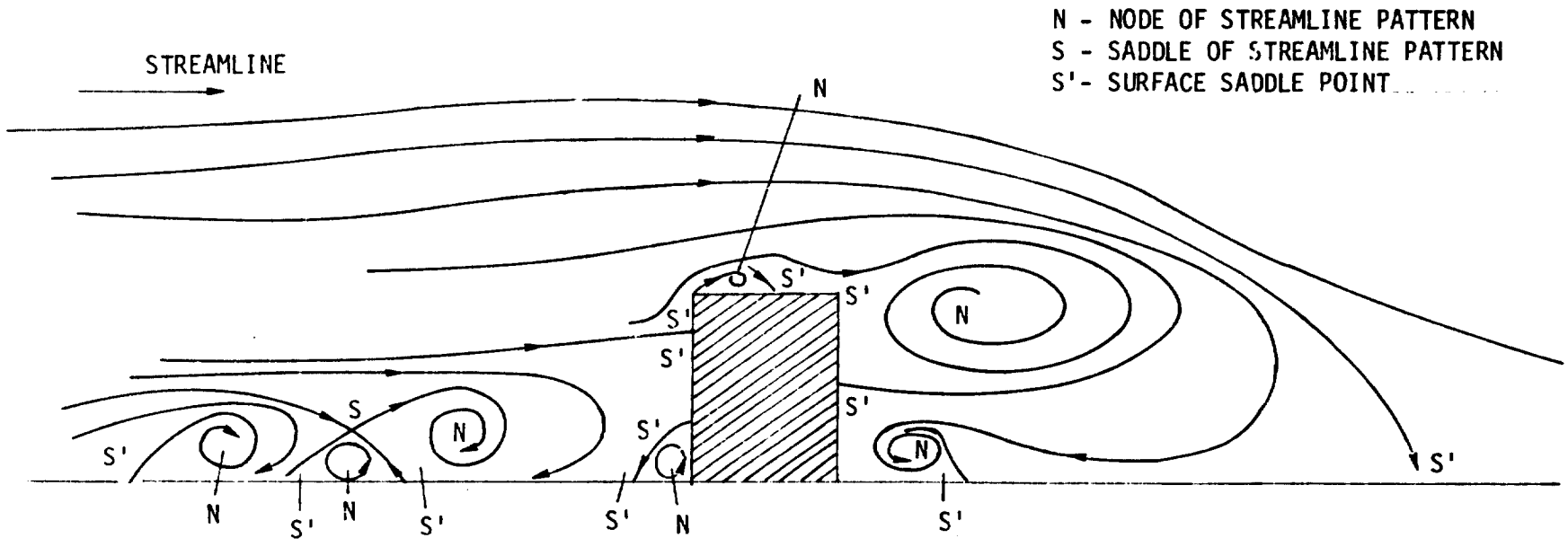

Figure 7. Postulated streamline pattern around a cube

$$\frac{u_s}{u_{s_{ms}}} = G\ (y/\delta) \tag{3}$$

$$\frac{u_n}{u_{s_{ms}}} = \tan \varepsilon_w\ g\ (y/\delta) G(y/\delta) \tag{4}$$

where u_n, u_s and $u_{s_{ms}}$ are the crossflow, streamwise, and free-stream velocities, respectively, and ε_w is the angle between the limiting streamline and the free-stream flow direction as previously defined (see Fig.3). G and g were assumed to be universal functions of y/δ and in general are only restricted by the boundary conditions:

$$y = \delta \quad G = 1,\ g = 0$$

$$y = 0 \quad G = 0,\ g = 1$$

ε_w is an unknown quantity that must be determined by the calculation method. Two representative models of the universal functions G and g are given by Mager[13] and Moore and Richardson[14]. Mager assumed two power functions of y/δ:

$$G = (y/\delta)^{1/n}\ , \qquad g = (1 - y/\delta)^2 \tag{5}$$

Moore and Richardson replaced the independent variables with y/θ_x and H_x as follows:

$$G = G(y/\theta_x,\ H_x)\ , \qquad g = (1 = y/(10\theta_x)^r \tag{6}$$

The main flow function G in equation (6) is similar to the formulation of von Doenhoff and Tetervin[15] for two-dimensional flows. The model of Moore and Richardson is more general than that of Mager in that a variable r replaces

the constant exponent in the expression for g. Although the models give good agreement with some experimental data, neither model adequetly represents all the data. One of the main difficulties with the Prandtl model is that it does not relate the physical influence of the main flow to the boundary layer. As shown by Squire and Winter[16], the development of crossflow is a direct result of the reorientation of vorticity due to the main flow. The Prandtl model does not explicitly include this effect.

Taylor[17] introduced the concept of dividing a skewed boundary layer into two parts - a collateral boundary layer near the surface with the velocity vectors in the direction of the wall shear stress, and a quasicollateral region further from the surface - joined by a transition region. A quasicollateral boundary layer is a skewed boundary layer that can be resolved into a collateral boundary layer by viewing from a moving coordinate system. Johnston[18] applied Taylor's model to establish four of the five auxiliary equations required to solve the momentum integral equations in streamline coordinates. The coordinate system used by Johnston is shown in Fig.8. Johnston formulated expressions for the two regions of the boundary layer as follows:

$$\frac{u_n}{u_{s_{ms}}} = u_s \tan \varepsilon_w \quad \text{for region I} \tag{7}$$

$$\frac{u_n}{u_{s_{ms}}} = \left(1 - \frac{u_s}{u_{s_{ms}}}\right) A \quad \text{for region II} \tag{8}$$

Note that the main-flow component, u_s, was explicitly included to account for the reorientation of vorticity due to main flow turning. When plotted in polar form, which Johnston was one of the first to use, the above expressions yield

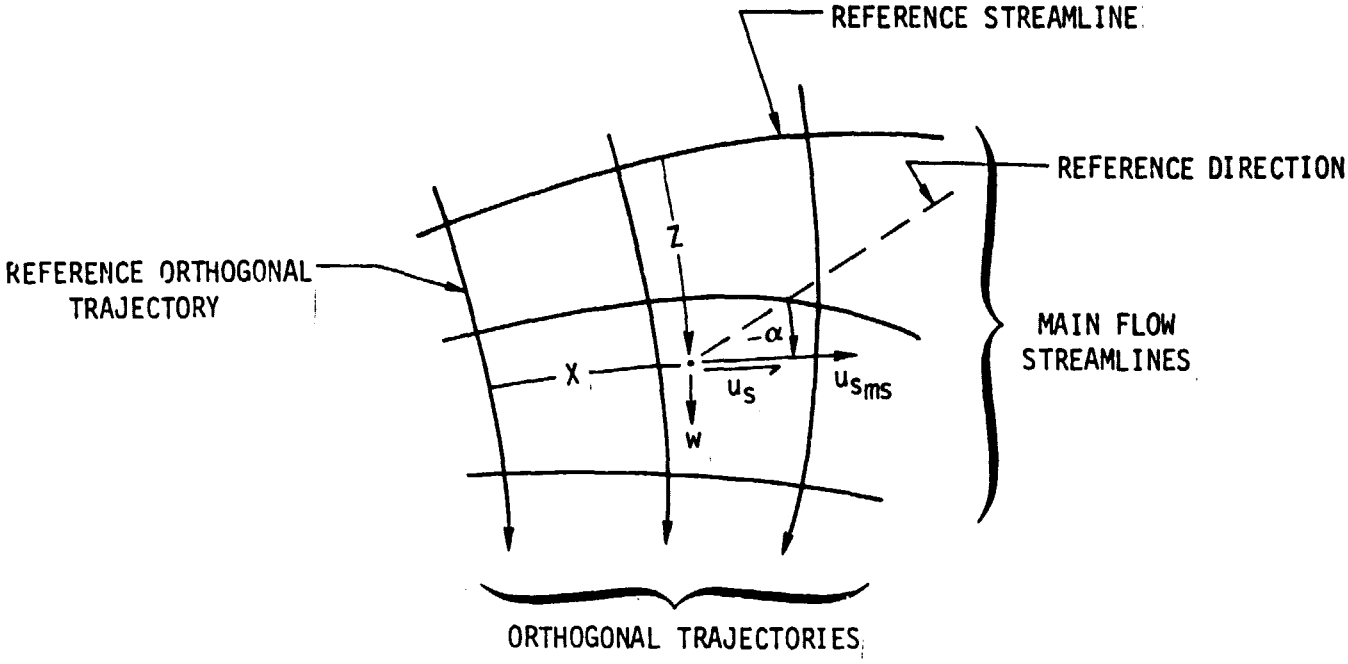

Note: Y axis points out of paper

Figure 8. Streamline coordinate system of Johnston

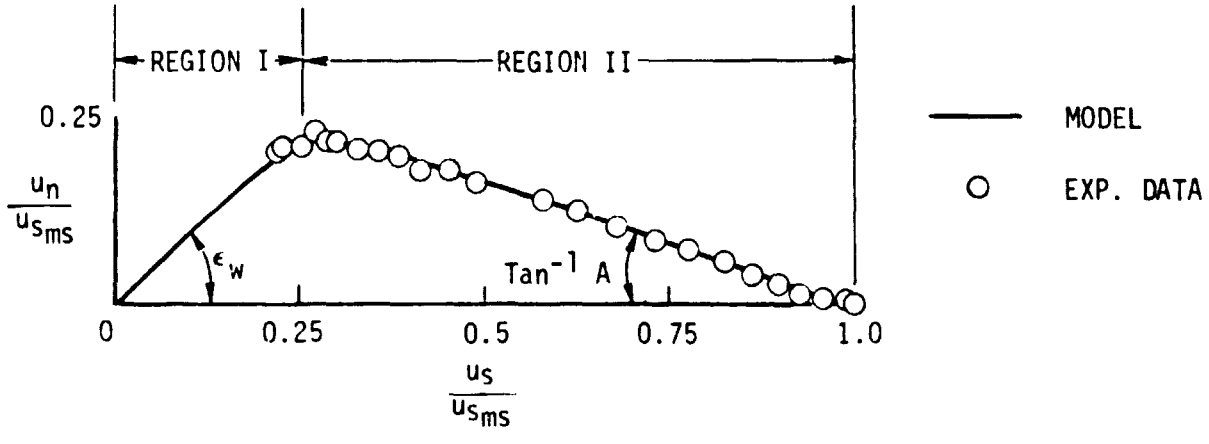

Figure 9. Johnson triangular polar plot

a triangular plot for the crossflow profile as shown in Fig.9. Regions I and II are separated by the apex of the triangle. This formulation does not include a transition region between the two parts of the boundary layer. Using the experimental configuration shown in Fig.10, in which a two-dimensional jet was forced to flow against a perpendicular back wall, and earlier experiments, Johnston found that the crossflow profile was represented quite accurately by the triangular model. One comparison between the triangular model and experimental data is shown in Fig.9. Johnston then formulated an analysis to solve the momentum integral equations using the triangular model in the following manner. He found that region II accounted for approximately 95-99 percent of the boundary layer thickness with the apex of the triangle falling between values of $u_\tau y/\nu$ of 12 and 16. Therefore, region I was assumed to lie in the laminar sublayer implying that the velocity profile in region I is linear. Furthermore, since the velocity vectors in region I were postulated to be collateral (see equation 3), two-dimensional boundary layer correlations, such as those developed by Clauser[19], or Ludweig and Tillman[20] with pressure gradients present, were used to determine the skin-friction coefficient. Finally, Johnston found that the angle of the inviscid portion of the triangular polar plot was related to the main-flow streamline angle relative to a fixed direction, α (see Fig.8), as follows:

$$A = -2u_{s_{ms}}^2 \int_0^{\alpha} \frac{d\alpha}{u_{s_{ms}}^2} \tag{9}$$

Using the above relationships, Johnston formulated four auxiliary equations so that a solution to the momentum integral equations could be obtained in parametric form. Fair to good agreement was obtained between the parameterized

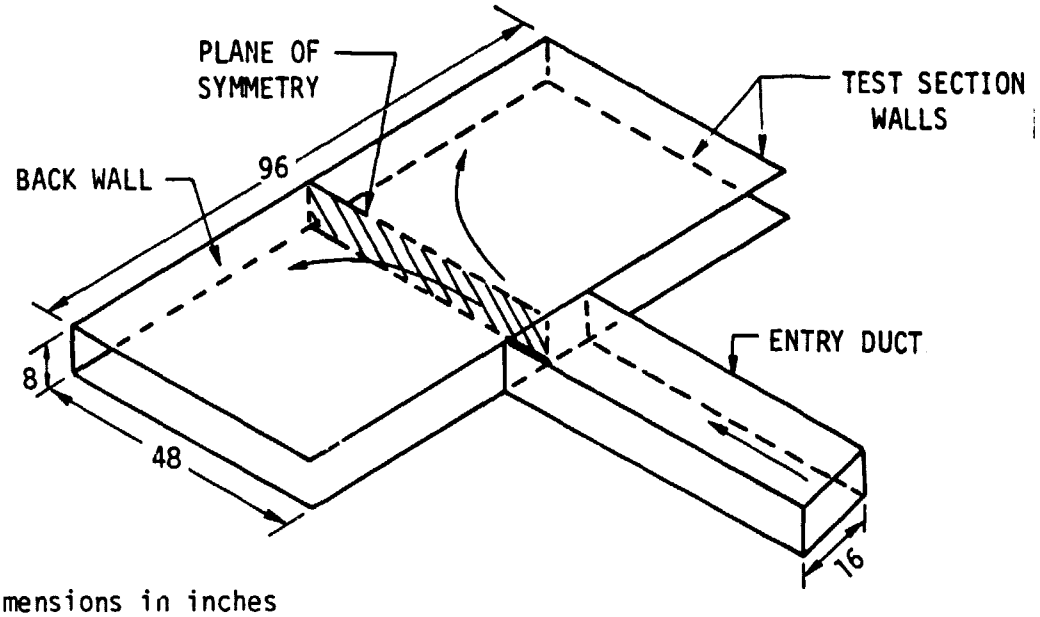

Figure 10. Experimental configuration of Johnston

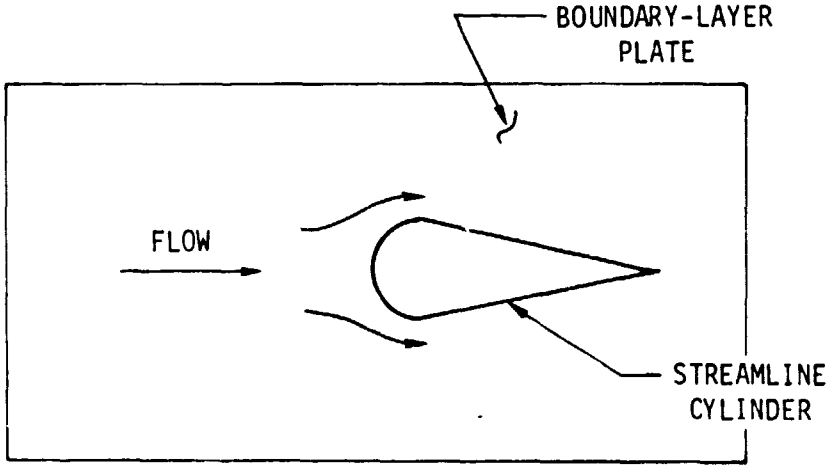

Figure 11. Streamline cylinder experimental arrangement

solution and his experimental data. Johnston was unable to determine a fifth auxiliary equation to close the solution. However, he indicated that the required equation involved a relationship between the streamwise velocity profiles and the other parameters involved in the solution scheme. No such formulation has been developed.

The triangular relationship between the crossflow and boundary-layer velocities can be based on theoretical grounds as indicated by Eichenberger[21]. In the layer near the surface, the wall viscous dissipation is very large and the boundary layer adjusts immediately to new conditions i.e. the free-stream flow inertia negligibly affects region I of the boundary layer so that a collateral velocity profile exists. In the outer layer, the skewed boundary layer depends on the history of the flow as do the flow phenomenon in an inviscid flow. Thus, in region II, viscosity plays a small role upon the secondary-flow velocity and Hawthorne's[22] inviscid secondary-flow theory can be applied which leads to a straight line velocity profile, in polar form, in region II. It must be emphasized, however, that Hawthorne's, and therefore Johnston's, models are only applicable for small crossflows. An explanation for the virtually nonexistant transition region between the two regions (Fig.9) is not obvious, but, as indicated by Eichenberger, the demarcation between the regions may be enhanced due to a two-layer turbulence phenomenon as developed by Townsend[23].

Johnston[24] applied the above analysis to predict the separation point in the plane of symmetry of his experiment. He again used correlations for skin friction that were derived for two-dimensional flows. Since on the plane of symmetry, the separation point is a singular point, Johnston identified the

separation point as the position where the axial component of the shear stress fell to zero. He found reasonable agreement between his analysis and the experimental results from his flow configuration, Fig. 10.

Hornung and Joubert[25] conducted an experiment to assess the validity of Johnston's triangular model. Their experimental configuration consisted of a streamlined cylinder mounted on a flat plate as shown in Fig. 11. They found that the triangular model was confirmed with good correlation. However, the value of yu_τ/ν at the vertex of the triangle was found to range up to 150 whereas Johnston found that this parameter ranged from 12 to 16 in his experimental data. Hornung and Joubert's work, then, contradicts the assumption made by Johnston that region I lies within the viscous sublayer. Since this assumption is the basis of much of Johnston's analysis, the validity of that analysis is questionable.

Even though these early experiments confirmed the triangular model, the triangular model has not proven to be universal. In particular, the outer region of the boundary layer cannot be universally represented by a straight line. Rather a crossover, crossflow polar plot, as shown in Fig. 12, represents the crossflow components for some flow conditions. This type of profile corresponds to a crossflow that reverses direction once through the boundary layer. Kliensich and Pierce[26] observed this type of flow on the endwall of the second bend in an S-turn duct. Langston[27] also observed this behavior in a turbine cascade passage. Eichelbrenner[28] described the crossover, crossflow plot by coupling the crossflow with the streamwise flow in polynomial form:

$$\frac{u_n}{u_{s_{ms}}} = \frac{u_s}{u_{s_{ms}}} \tan \epsilon_w \left[1 + c_1 \left(\frac{u_s}{u_{s_{ms}}}\right) + c_2 \left(\frac{u_s}{u_{s_{ms}}}\right)^2 + \cdots\cdots\right] \quad (10)$$

where c_1 c_2 ... are evaluated from boundary conditions at the edge of the boundary layer and at the wall. By using enough terms, equation (10) can be used to describe

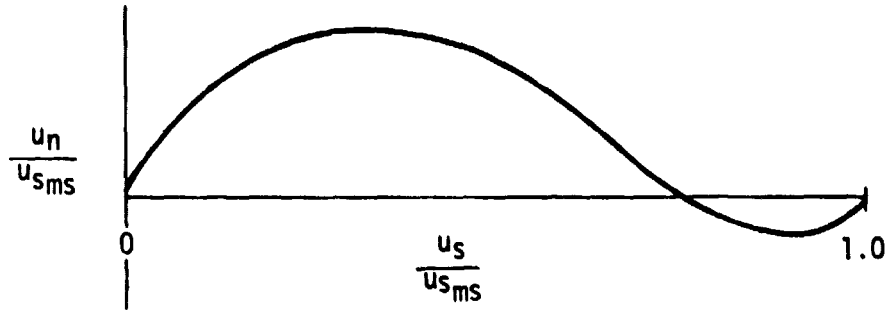

Figure 12. Crossover, crossflow polar plot

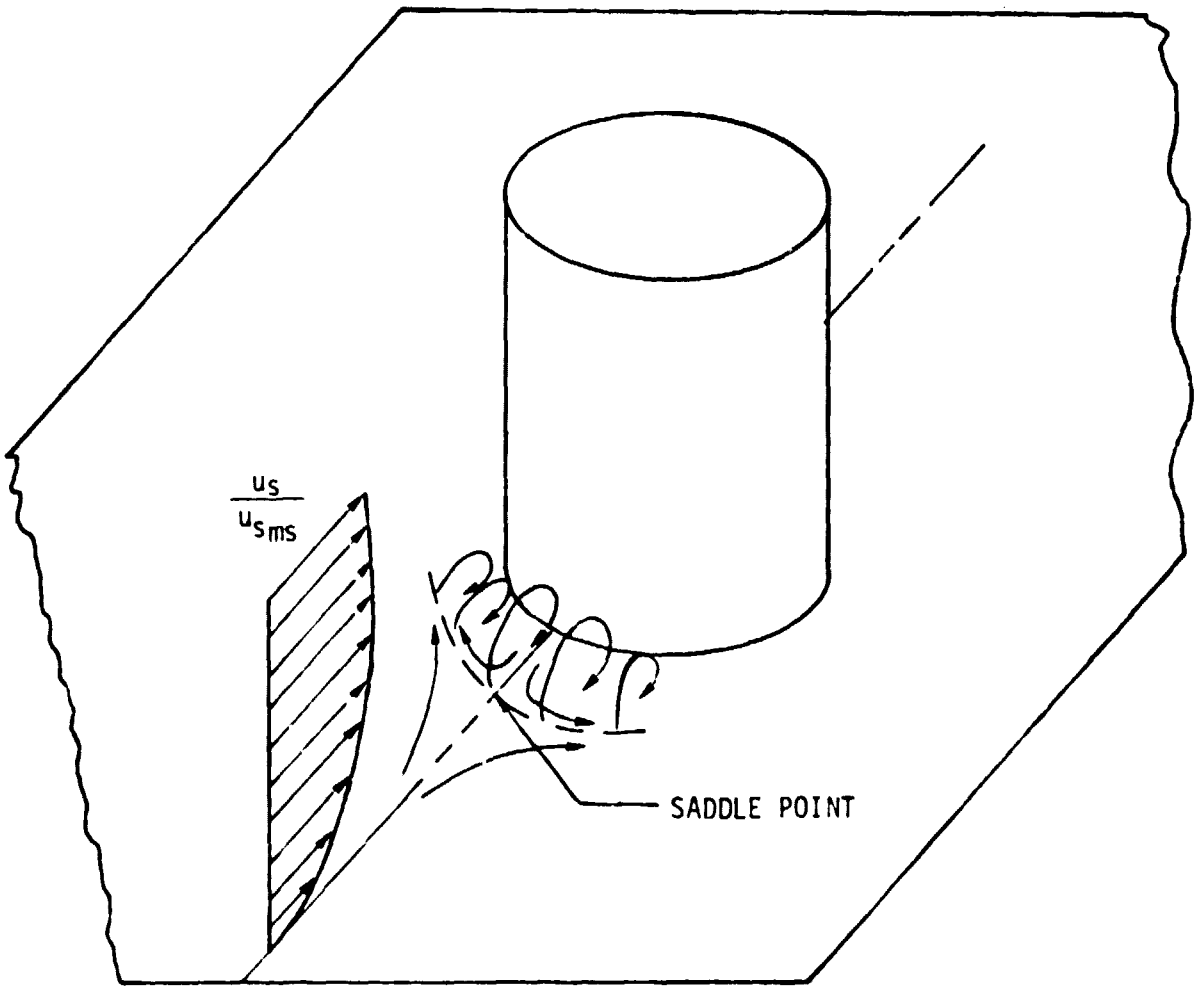

Figure 13. Formation of a symmetrical horseshoe vortex around a single cylinder mounted on an endwall

almost any kind of crossflow. Alternatively, Langston[27] found that the following expression correlated the turbine cascade data:

$$\frac{u_n}{u_{s_{ms}}} = \tan\left[\varepsilon_w - a\, z\right) e^{-\gamma z}] \qquad (11)$$

where a is a crossover, crossflow coefficient, γ is a crossflow strength coefficient, and z is the distance from the endwall surface normalized by the airfoil axial chord length. In Langston's representation, a Johnston-like polar plot is obtained for $a = 0$, $\varepsilon_w \geq 0$, and $\gamma > 0$. For values of $a > 0$, $\varepsilon_w > 0$, and $\gamma > 0$, equation (11) yields crossover, crossflow plots. Equation (11) has three experimentally determined constants and is no more general than a third degree polynominal as proposed in equation (10). In addition, neither of the above two approaches can be predictive unless an approximation for the spanwise variation of the streamwise velocity component can be made. Such an approximation for three-dimensional flows apparently does not exist according to Nash and Patel[1] and Langston[27].

Based on the above analysis, no general universal crossflow profile has been found. Johnston[29] concluded that the flow in three-dimensional boundary layers is dependent in each case on boundary conditions and flow history. Since integral methods to solve the boundary layer equations require a crossflow profile, Wheeler and Johnston[30] concluded that three-dimensional prediction methods using integral techniques cannot be general enough to be applied to a variety of geometric conditions. However, although the crossflow boundary layer approach and polar plot cannot be used in a predictive fashion, Langston[27] has shown that this approach provides a useful and simple picture of a three-dimensional boundary layer which is not conveyed by other representations.

With the abandonment of using integral techniques to provide general solutions to the three-dimensional boundary-layer equations, methods which use finite difference approximations to the differential boundary layer equations are being widely explored. To date emphasis has been placed on developing models for duct flows: Pratap and Spalding[31], Briley and MacDonald[32], and Dodge[33], or for flows with a laminar boundary: Ghia, et al.[34] and Briley and MacDonald[35]. Only one technique, that of Briley and MacDonald[36], has been developed to predict a general three-dimensional turbulent flow with a significant crossflow component as exists in a turbine cascade. They developed solutions for the flow past both swept and unswept leading edges and compared their predictions with the experimental results of Shabaka[37], who obtained measurements for an unswept leading edge at zero incidence. Shabaka's measurements, which were the only detailed measurements of secondary flow that Briley and MacDonald could find, were taken in the corner flow region, well downstream of the leading edge, where the secondary flows were relatively weak. Briley and MacDonald[36] found that the measured crossflows were ten times greater and of opposite sense from the predicted flows. Due to a lack of upstream information, especially near the separation point, Briley and MacDonald could not assess the cause of the discrepancy between experiment and theory.

The dearth of detailed experimental data for turbulent flows with strong secondary components, as encountered by Briley and MacDonald[36], has been the subject of the recent Stanford Conference on Complex Turbulent Flow. Although some measurements exist, as discussed below, they cannot be used for computer code assessment. In order for an experimental data set to be used for code assessment, the data must consist of profiles of mean and turbulence quantities at upstream and downstream positions, as well as at various locations around the body

which generates the secondary flow. Such a comprehensive data set does exist in the open literature.

One configuration which has been used to obtain data with strong secondary flows is flow past a single cylinder mounted on a flat plate. The boundary layer upstream of the cylinder undergoes a three-dimensional separation due to the strong adverse pressure gradient imposed by the presence of the cylinder as shown in Fig. 13. The separated shear layer creates a saddle point on the axis of symmetry and rolls up to form a vortex whose ends are swept downstream around the base of the cylinder. When viewed from above, this vortex has the characteristic horseshoe-like shape. Investigation of the end-wall separation in front of an isolated single cylinder is an attractive experiment because the strong cross-flow can be analyzed without the added complication of an asymmetric flow as exists in a cascade passage and shown by Langston, et al.[38].

However, none of the experiments reported in the literature on the endwall separation in front of a single cylinder contain a data set applicable for code assessment. Ram[39] carried out detailed measurements in front of a 15 cm diameter cylinder at a Reynolds number based on the cylinder diameter, Re_D, of 4.1×10^5. Ram measured static pressures on the endwall and cylinder surfaces and carried out five-hole probe measurements. However, none of the five-hole probe measurements were carried out near the separation point, which is critical to code assessment as pointed out by Briley and MacDonald[36]. Belik[40] studied the horseshoe vortex system associated with cylinder diameters of 2, 3, 4, and 6 cm for $0.36 \times 10^5 \leq Re_D \leq 2.2 \times 10^5$. However, his experiment was designed primarily for flow visualization, and only minimal endwall static pressure data along the axis of symmetry in front of the cylinder was obtained. Both Hornung and Joubert[25], mentioned previously, and East and Hoxey[41] made detailed boundary layer measurements

upstream of a streamlined cylinder, as shown in Fig. 11. Hornung and Joubert measured static pressures and flow direction using a yaw meter upstream of a 56 cm diameter streamlined cylinder at $Re_D = 6.5 \times 10^5$. However, only limited data was taken downstream of the separation line, and none was taken near the saddle point. East and Hoxey measured the flow ahead of a 61 cm diameter streamlined cylinder at $Re_D = 3.7 \times 10^6$. They carried out extensive flow field measurements obtaining velocity profiles and flow direction with a 3-hole probe (no pitch), static pressure distributions, and skin friction. They made measurements ahead of and around the side of the model, but they did not make any detailed measurements downstream of the separation line or near the saddle point. Baker[42] carried out an extensive program, looking at the separation in front of a number of cylinders over a range of Reynolds numbers for both laminar and turbulent boundary layers. However, he only recorded static pressures on the endwall and cylinder surfaces. No probing was accomplished to characterize the flow field. His work did point out, however, the significantly different flow field associated with separation of laminar and turbulent three-dimensional boundary layers. In the case of laminar flow, various numbers of vortices existed in front of the cylinders on the axis of symmetry. The number of vorticies depended on the flow velocity and cylinder diameter. In addition, the entire vortex system oscillated in a periodic manner above a certain flow speed. A periodic motion of this type was not observed with a turbulent boundary layer, but rather oscillations about a mean flow condition were observed. The mean flow pattern was not affected by the flow velocity in the turbulent regime. Therefore, measurements of secondary flows in a laminar boundary layer, such as those of Peake and Galway[43], are not applicable to turbulent boundary layers. Taniguchi et al.[44] also studied the flow

around a single cylinder mounted to a flat plate. However, they were mainly concerned with the drag force on the cylinder and did not obtain detailed flow measurements upstream of the cylinder.

Another configuration that has been used to obtain flow measurements in a symmetric three-dimensional boundary layer is similar to that used by Johnston[18,24] shown in Fig. 10. Mojola[45] measured mean velocity profiles, static pressure profiles, and flow angles in the central plane of such a model. Unfortunately, the flow stability in this experiment was such that the flow was significantly altered by the presence of probes. Thus the data can only be used in a qualitative sense.

Experimental Model and Wind-Tunnel Modifications

Design

As previously defined, there are two goals of this experiment: to obtain a data set that can be used for three-dimensional numerical computer code assessment, and to further elucidate the characteristics of the vortex system that is formed in front of a cylinder mounted on a flat plate. These goals will be accomplished by obtaining detailed flow measurements in the vicinity of a single isolated cylinder. The measurements will include static pressures on the endwall and cylinder surfaces, extensive five-hole probe pressures in front of and around the cylinder, and velocity fluctuations using a hot wire where the flow is steady enough to yield meaningful results. These experiments will be conducted in the NASA two-cylinder, low-speed wind tunnel shown in Fig. 14. A description of this facility is given by Langston[46-50]. The tunnel, however, must be modified to accomodate a single large-diameter

Figure 14. Overall view of NASA two-cylinder, low-speed wind tunnel

cylinder and the required endwall static pressure taps. A discussion of the designed modifications to the tunnel follows.

The wind-tunnel test section is one foot high and six feet wide. The test section height and entrance conditions were designed so that two separate turbulent boundary layers can develop on the top and bottom endwalls. With the cylinder mounted vertically in the tunnel and spanning the tunnel height, individual flow separations will exist on each endwall. However, as indicated by Langston[49,50], the flow entering the test section is not perfectly symmetric from top to bottom. To avoid any uncertainty, all detailed boundary layer measurements will be made near one endwall. The decision as to which boundary layer to characterize was based on the desire to use the existing probe positioning device, described by Langston[50], which attaches to the tunnel ceiling. Since the probes used in the test program will be cantilevered from the ceiling, probe interference effects will be much larger on the ceiling boundary layer than on the floor boundary layer. Characterization of the tunnel floor boundary layer, then, is the proper choice to minimize probe interference effects. Therefore, the floor of the test section has been designed to serve as the instrumented endwall. The floor will consist of a support plate, Fig. 15, and a mating instrumented disk shown in Fig. 16. The support plate will be bolted to the existing test section frame, and the instrumented disk will be concentrically clamped to the underside of the support plate with sealing provided by an O-ring. The clamping arrangement will consist of four toggle clamps and four cam followers equally spaced around the disk. The cam followers will be mounted into slides, as shown in Fig. 17, so that the instrumented disk can be easily retracted from the support plate and rotated to any desired angular location.

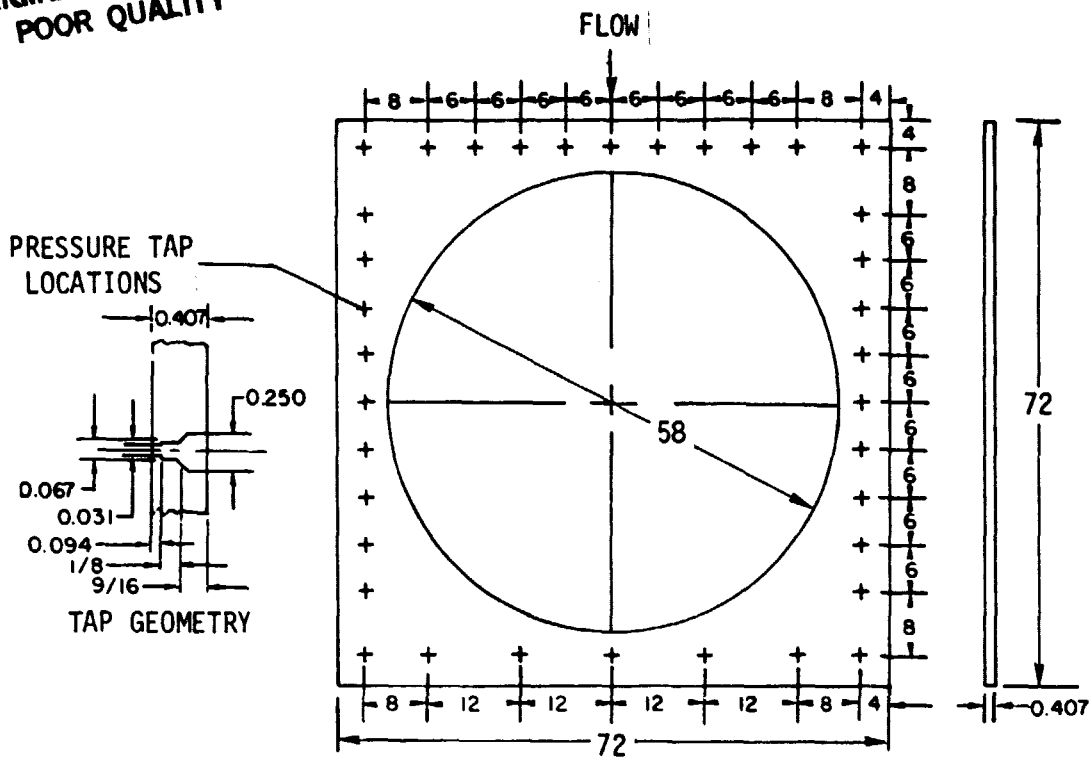

Dimensions in inches

Figure 15. Wind tunnel floor support plate

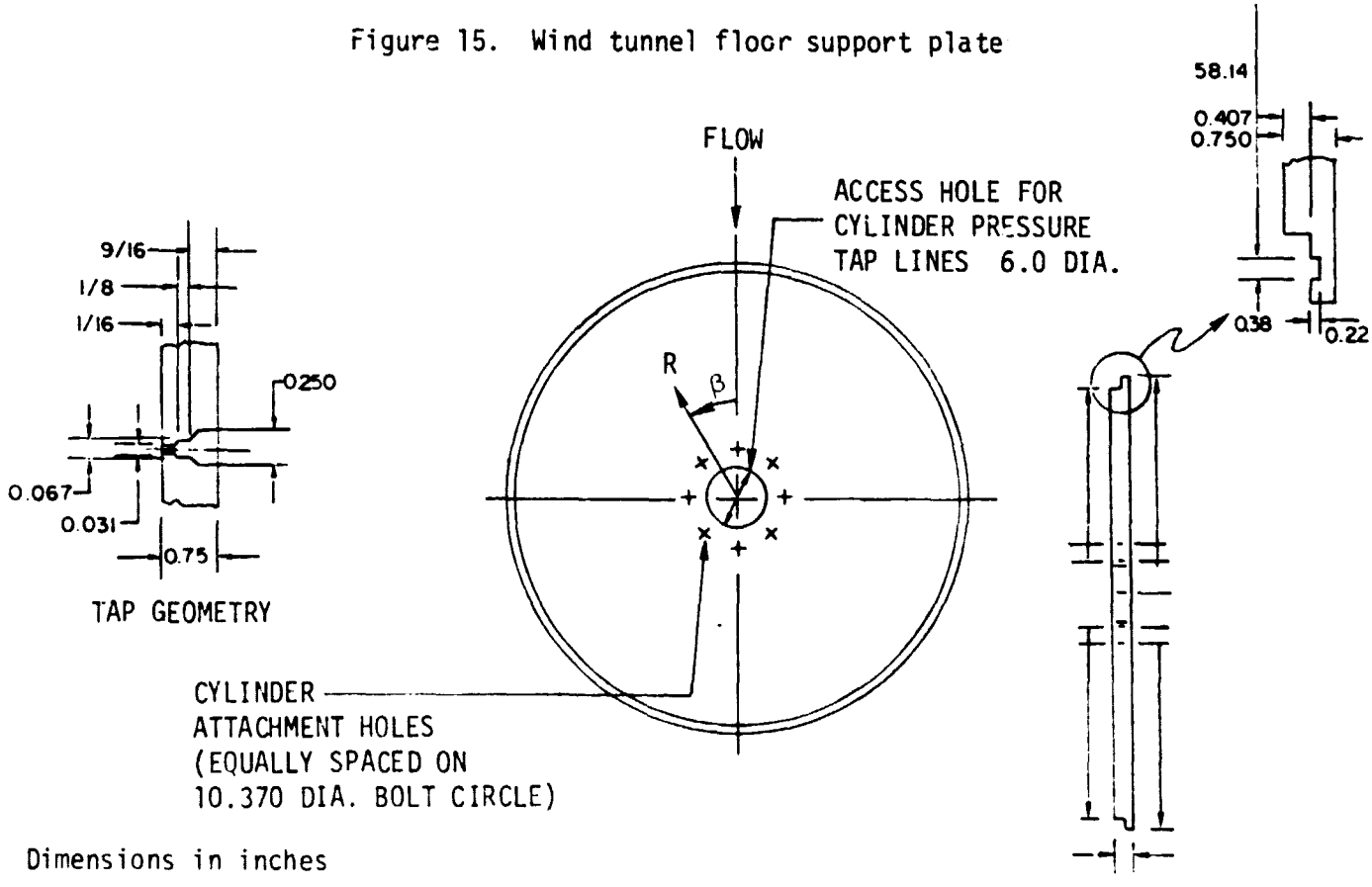

Dimensions in inches

Figure 16. Wind tunnel floor instrumented disk (See Table I for tap locations)

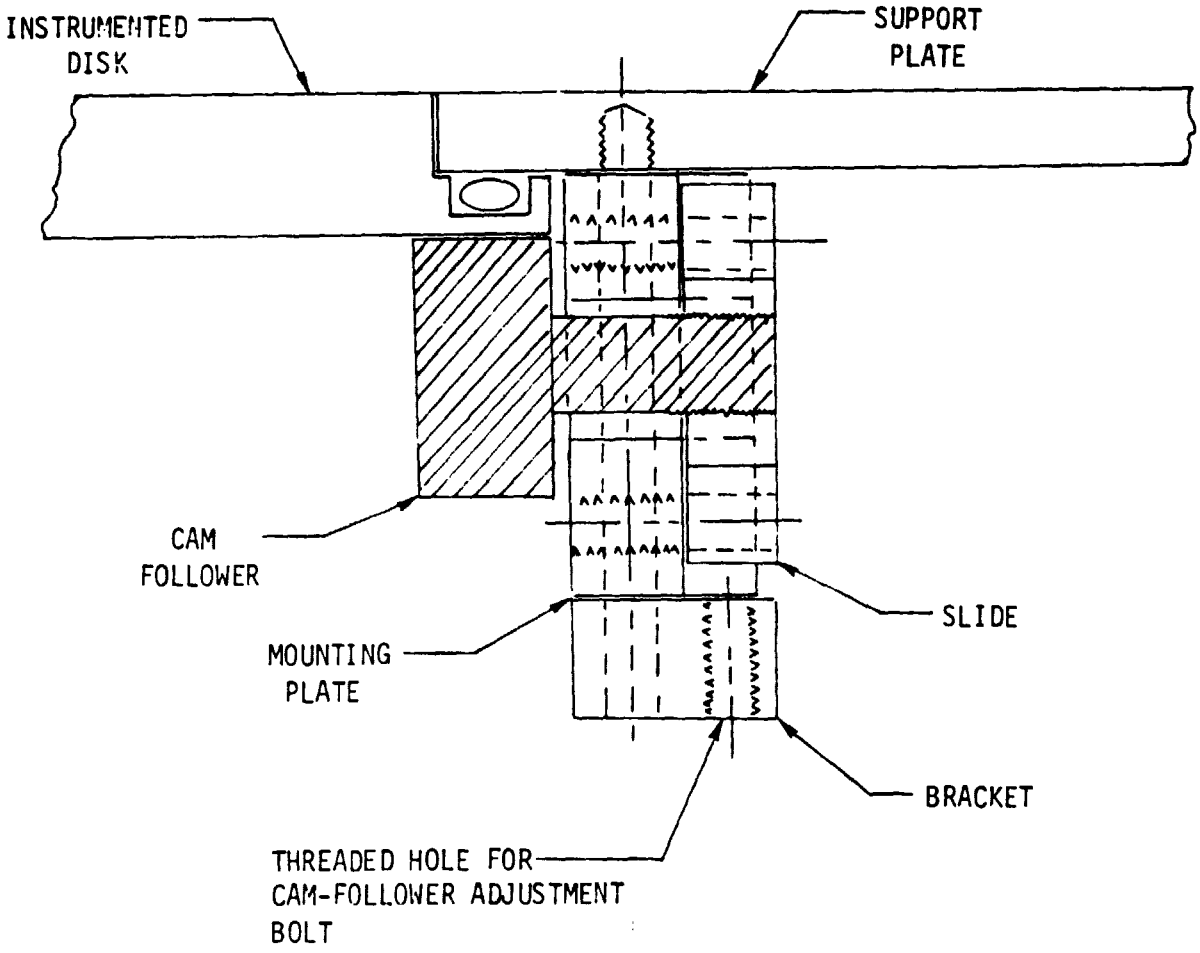

Figure 17. Cross-sectional view of cam-follower slide assembly

The procedure for retracting the disk will involve first releasing the toggle clamps so the disk will rest on the cam followers. Then by retracting the bolts tnat hold the slides as shown in Fig. 17, the cam followers will be lowered until the O-ring seal clears the support plate. The disk can then be rotated on the cam followers as required. The disk will be reinserted into the support plate by reversing the above retraction procedure. This design will enable detailed endwall static pressure measurements to be obtained, with a minimum number of pressure taps installed in the disk, by sequentially rotating the disk to position the pressure taps at desired angular locations.

The pressure tap locations on the instrumented disk are contained in Table I. Pressure taps have been staggered along the disk radius at angular locations of β = -10, 0, 10, and 20 degrees. The tap locations along these radii are arranged so that at a given angular location, pressures can be measured along a radial line every 0.25 inch for $6 \leq R \leq 14$, every 0.50 inch for $14 \leq R \leq 20$, and every 1.00 inch for $20 \leq R \leq 28$, where R is the radius in inches from the disk center, by successively rotating each of the four lines of taps to the angular location. Additional taps have been included on the instrumented disk so that a general survey of the endwall static pressure distribution can be obtained without rotating the disk. Static taps will also be machined into the support plate at locations shown in Fig. 15. These taps will be used for defining boundary conditions.

The diameter of the test model (cylinder) was chosen based on a trade-off between desiring a large-diameter cylinder to minimize probe effects and desiring a small-diameter cylinder to reduce the interference effects of the tunnel sidewalls. As a result of this trade-off, a nominal cylinder diameter of 12 inches was chosen. This diameter is large enough so that the model scale is 100 times larger than the characteristic dimension of a typical five-hole probe or hot

wire, which is on the order of 0.1 inch. Based on inviscid calculations, the interference between a one-foot diameter cylinder and the tunnel sidewalls is expected to increase the pressure coefficients on the cylinder surface by only several percent, which is believed to be acceptable.

A sketch of the test model is shown in Fig. 18. The cylinder will be machined from commercially available aluminum tubing with a nominal outer diameter of 12 inches and a nominal wall thickness of 1 inch. Because of loose tolerances on tubing concentricity and wall thickness, the cylinder was designed with an outer diameter of 11.75 inches to guarantee a uniform circular diameter. The height of the cylinder will be nominally 12 inches to match the test section height.

The cylinder will be concentrically located and bolted on the instrumented disk via the through holes in the disk shown in Fig. 16. O-rings will be used to seal between the cylinder and the floor and ceiling of the tunnel. The cylinder will rotate with the disk so that detailed static pressure distributions on the cylinder surface can also be measured with a minimum number of pressure taps on the cylinder. The tap locations on the cylinder are given in Table II. Pressure taps will be staggered along the cylinder axis at four angular locations (which will be aligned with the four radial lines of staggered taps on the instrumented disk during assembly) so that static pressures can be measured every 0.25 inch on the bottom half of the cylinder at any angular location. Additional taps have been included to enable a survey of the cylinder surface static pressures to be obtained without rotating the cylinder and to check flow symmetry along the cylinder axis. The lines connected to the pressure taps on the cylinder will be routed through the access hole in the center of the instrumented disk (Fig. 16) so as not to interfere with the probe positioning device located on the test-section ceiling. Thus, modification of the tunnel ceiling will not be required.

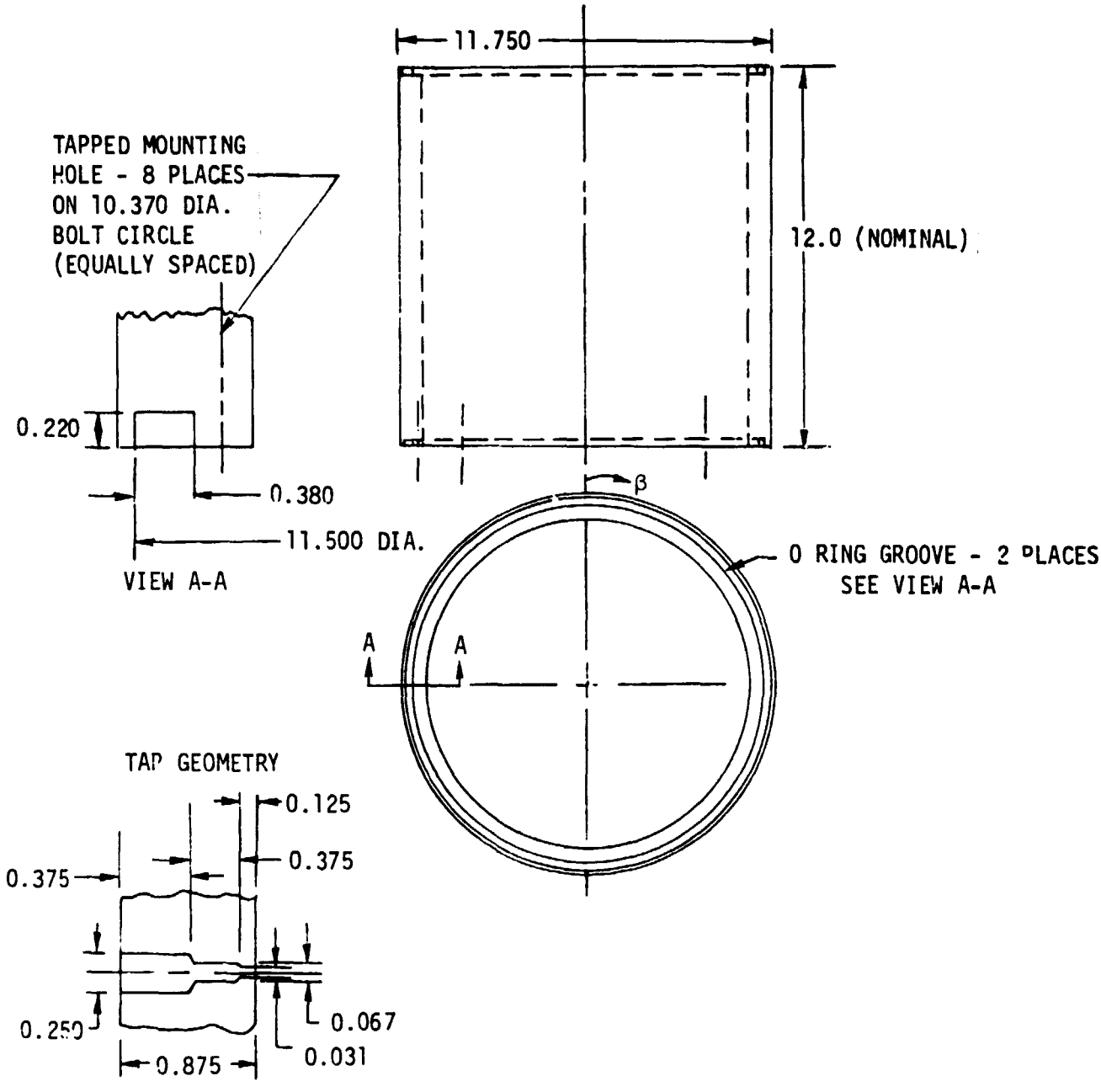

Figure 18. Cylinder test model (See Table II for static tap locations)

Fabrication and Installation

The test cylinder and the parts for modifying the tunnel test section are partially fabricated. The support plate has been machined but the pressure tap holes and mounting holes for the clamps and cam follower slide assemblies have not been installed. The instrumented disk has been fabricated with the pressure tap holes and through holes to mount the cylinder to the disk installed. The access hole at the disk center for routing out the cylinder pressure tap lines has not been machined. A plug to fill the access hole will also be fabricated. This plug will be installed for tests with the cylinder not installed. The test cylinder has been turned down to the correct outer diameter, the pressure tap holes machined in the cylinder wall, and the O-ring groove and the threaded bolt holes on the cylinder bottom surface installed. The cam-follower slide assemblies are in the process of being fabricated.

After completing the fabrication indicated above, the test configuration will be assembled as follows. The wind-tunnel test section will be detached from the tunnel and located in the shop assembly area. The existing floor, including two of the angle iron supports that would interfere with the instrumented disk pressure tap lines, and sidewalls will be removed. The support plate will be mounted onto the test section frame and the mounting hole locations will be transferred to the plate from the frame. The support plate will be installed using shims to level the plate and locate it 12 inches from the test-section ceiling. The instrumented disk will be clamped to the support plate taking care to minimize steps on the inside surfaces. The precise distance between the center of the disk and the tunnel ceiling will be measured with the probe positioning device in place on the tunnel ceiling. The test cylinder will then be cut to the appropriate length, and the

O-ring groove will be machined into the top surface. After installing the pressure tap lines into the cylinder, the cylinder will be bolted to the instrumented disk with the cylinder pressure tap holes properly aligned with those on the instrumented disk. After reassembly of the sidewalls, which will involve tapping mounting holes in the support plate, the test section will be installed into the wind tunnel for testing.

Five-Hole Probe Calibration

Two five-hole probes, United Sersor Model DC-.093-24-F-22, are available for use in this program. The geometry for the probes is shown in Fig. 19. The probe tips have a diameter of 0.095 inch instead of the stock configuration of 0.125 inch. In addition, the tips are ogival rather than a truncated cone as in the stock configuration, since it was found that the corners of the truncated cone, even though they contain large obtuse angles, cause inconsistencies in the calibration. (See Camarata et al.[51].) The ogival tip makes the probe calibration less sensitive to changes in Reynolds number. The tip of the probe is aligned with the shaft axis (which is the reason for the "shephard's crook") so that as the probe is rotated about the shaft axis the tip does not move. The nomenclature for the pressure taps is shown in Fig. 19. Tap 1 is the impact pressure while taps 2 and 3 are for nulling the probe in yaw , and taps 4 and 5 are for dynamic pressure and pitch.

The probes were calibrated in an air jet issuing from a 1.5 inch diameter nozzle. The calibrations were accomplished at a dynamic head of approximately 2.6 inches of water. The sign convention used for the calibration tests is shown in Fig. 20. Yaw angle, β, was defined as the angle between the plane formed by the tip and the shaft of the probe and the projection of the velocity vector on the

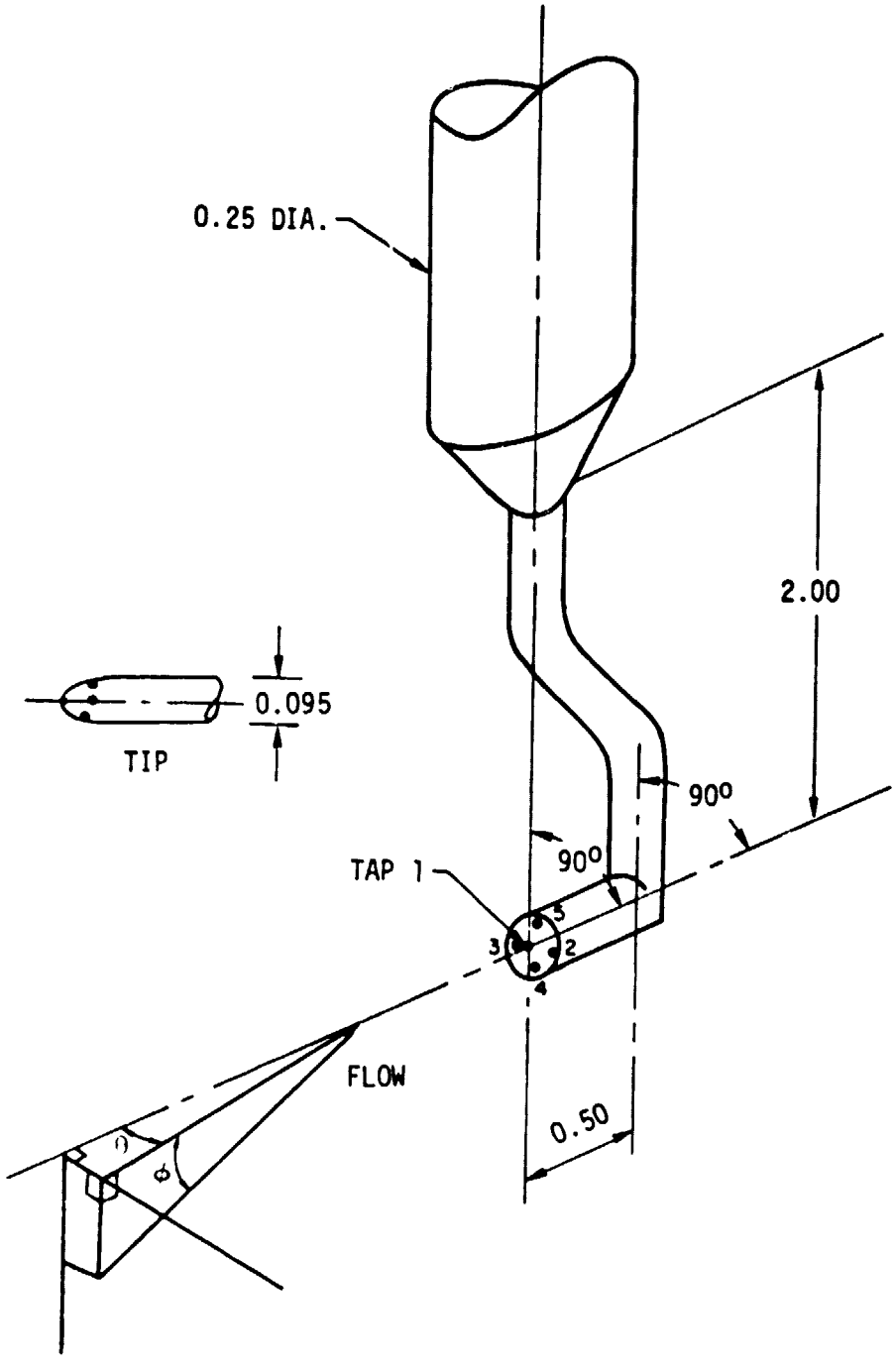

Figure 19. Five-hole probe configuration

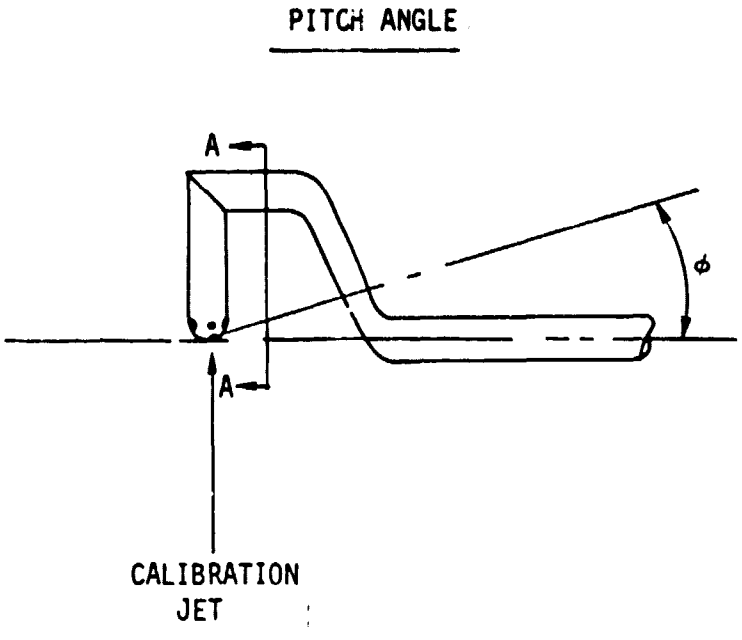

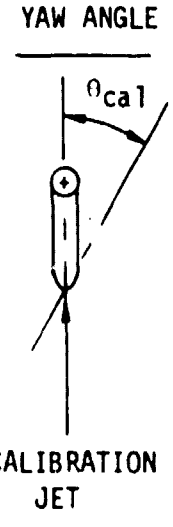

Figure 20. Sign conventions for five-hole probe calibration

plane perpendicular to the shaft. Pitch angle ϕ was defined as the angle between the velocity vector and the plane perpendicular to the probe shaft. The probes were calibrated over a range of pitch angles from -29 to +30 degrees. For each calibration condition, the probes were nulled in yaw by turning the probe about the shaft axis until P_2 equaled P_3. The resultant yaw angle, as measured relative to a flag mounted on the shaft, was recorded as θ_{cal}. The pressures from the remaining taps were also recorded, and the calibration curves shown in Fig. 21 were generated.

Measurements will be acquired in the wind tunnel in a similar manner. At a given spatial location in the flow field, the probe will be rotated until the pressures from taps 2 and 3 are equal. The probe rotation will be measured relative to a laser alignment beam and designated θ_{meas}. The sign convention for θ_{meas} will be that shown in Fig. 19. The pressures P_1, P_4, and P_5 will be recorded. The data will be reduced as follows. The pressure ratio $(P_4 - P_5)/(P_1 - (P_4 + P_5)/2)$ will be calculated from the measured data and the pitch angle, ϕ, determined from Fig. 21A. Knowing ϕ, the parameter $(P_1 - (P_4 + P_5)/2)/q$ will be determined from Fig. 21B and used to calculate the local dynamic pressure, q. Also using ϕ, the parameter $(P_T - P_1)/q$ will be obtained from Fig. 21C in order to calculate the total pressure. Similarly, the calibration yaw angle, θ_{cal}, can be extracted from Fig. 21D. The flow yaw angle, θ, then is the sum of θ_{cal} and θ_{meas}. Local static pressure will be calculated from the total and dynamic pressures using the Bernoulli equation. The direction of the velocity vector will be defined by the angles ϕ and θ.

Data Acquisition System

An ADAC Corporation data acquisition system will be utilized for acquiring experimental data. The system includes a Digital Equipment Corporation (DEC)

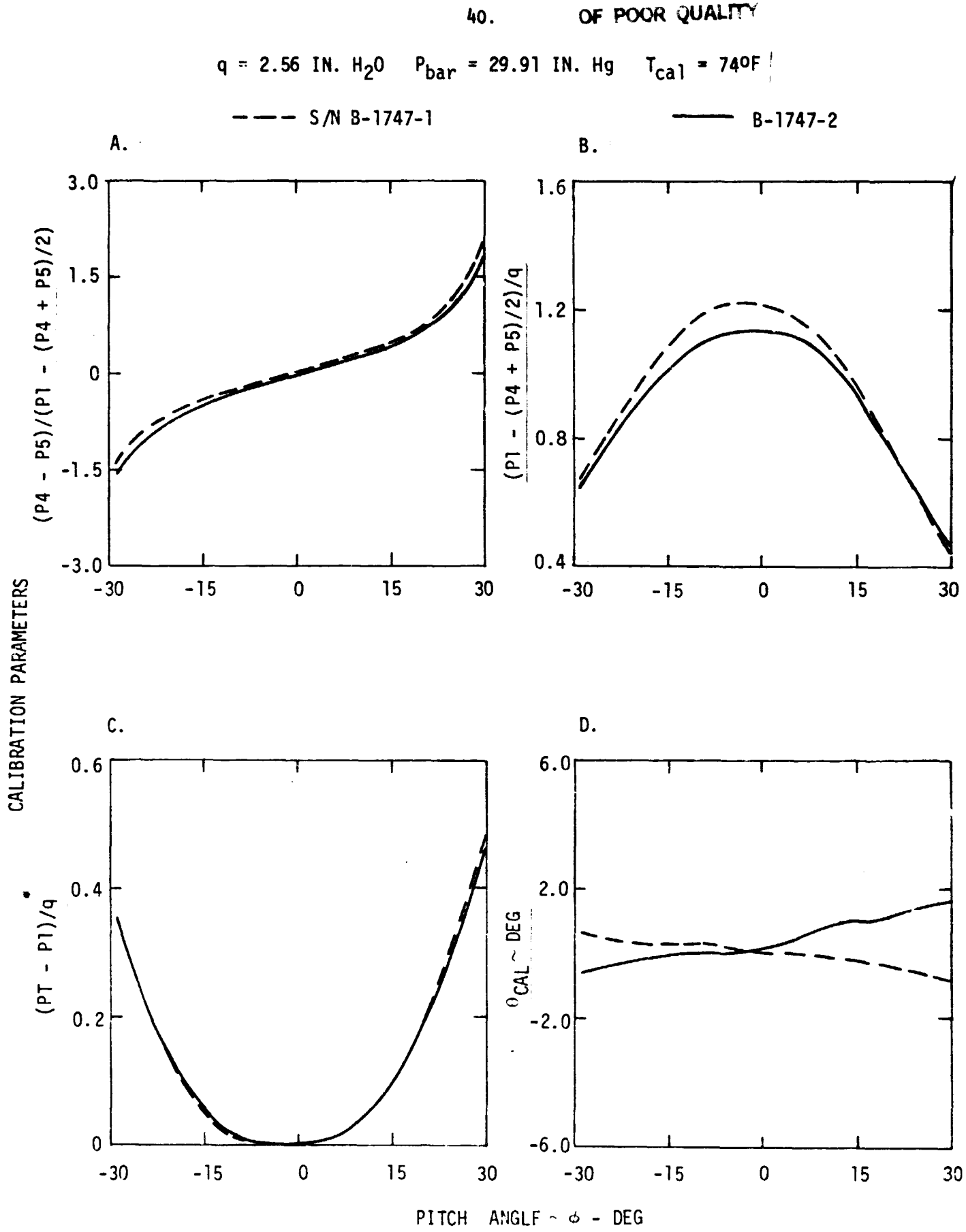

Figure 21. Five-hole probe calibration curves

LSI 1102 microcomputer with 32K words memory, the DEC RT-11 operating system, a DEC VT 100 terminal, ADAC dual 8 inch floppy disk drives, ADAC analog to digital and digital to analog convertors with software support packages, and an Axiom IMP miniprinter. The intent is to use the data acquisition system to acquire the data and reduce it to engineering units for on-site analysis. The system will also be used interactively with the main-frame computer, an IBM 3081 model D, to transfer the data to the main frame for reduction. In this application the data acquisition system will act as a remote terminal to the main frame. In order to utilize the data acquisition system in the above manner, software packages will be developed for acquiring the experimented data, a communications package will be developed for linking the data acquisition system to the main frame, and additional software packages will be written to reduce and assemble the data using the main frame.

Saddle Point Model

The Oswatitsch model for singular points in a flow was extended to cover the case of an asymmetric saddle point. The first draft of a final report on this analytical model was completed and is now being rewritten. Work is also underway to write a paper on the analysis.

Acknowledgements

The work reported on here was carried out by Mr. Wayne A. Eckerle, a doctoral candidate in the Mechanical Engineering Department and by the principal investigator. Mr. Craig Wagner, a masters candidate in the Department, worked on the Oswatitsch model with the principal investigator.

TABLE I

INSTRUMENTED DISK STATIC PRESSURE TAP LOCATIONS

R IN β-DEG	-20	-10	0	10	20	±40	±60	±80	90
	9.75	6.25	5.90	6.50	6.75	9.00	9.00	9.00	9.00
	12.75	7.25	7.00	7.50	7.75	12.00	12.00	12.00	12.00
	15.50	8.25	8.00	8.50	8.75	15.00	15.00	15.00	15.00
		9.25	9.00	9.50	9.75				
		10.25	10.00	10.50	10.75				
		11.25	11.00	11.50	11.75				
		12.25	12.00	12.50	12.75				
		13.25	13.00	13.50	13.75				
		14.50	14.00	15.00	15.50				
		16.50	16.00	17.00	17.50				
		18.50	18.00	19.00	19.50				
		21.00	20.00	22.00	23.00				
		25.00	24.00	26.00	27.00				
			28.00						

TABLE II

TEST CYLINDER STATIC PRESSURE TAP LOCATIONS

Z IN / β-DEG	-20	-10	0	10	20	±40	±60	±80	90
	1.50	0.125	1.00	0.75	0.50	2.00	2.00	2.00	6.00
	3.50	1.25	2.00	1.75	1.50	4.00	4.00	4.00	
	5.50	2.25	3.00	2.75	2.50	6.00	6.00	6.00	
		3.25	4.00	3.75	3.50	9.00		9.00	
		4.25	5.00	4.75	4.50				
		5.25	6.00	5.75	5.50				
		9.00	7.00	9.00	9.00				
			8.00						
			9.00						
			10.00						
			11.00						

Nomenclature

A - parameter related to the angle of the inviscid portion of Johnston triangular polar plot

a - constant in Langston polar-plot relationship, equation (11)

c - constant in Eichebrenner polynomial polar-plot relationship, equation (10)

G - function for crossflow profile, equations (3) and (4)

g - function for crossflow profile, equation (3)

H_x - δ_x/θ_x boundary layer shape factor

J - Jacobian of the shear-stress vector

n - related to the shape factor, $H_x = (n + 2)/n$

P_1-P_5 - five-hole probe pressures, Fig. 19

Q - resultant velocity

R - radial location of static pressur taps

r - exponent in Moore and Richardson crossflow relationship, equation (6)

Re_D - Reynolds number based on the cylinder diameter

u - axial velocity

u_n - crossflow velocity

u_s - streamwise velocity

u_τ - friction velocity = square root of the quanity wall shear stress divided by the density

w - transverse velocity

x,y,z - streamline coordinate system, Fig. 8

α - main-flow streamline angle relative to a fixed direction, Fig. 8

β - angular location of static pressure taps

Λ - divergence of the shear-stress vector

γ - crossflow strength coefficient, equation (11)

δ - boundary layer thickness

Nomenclature (Continued)

δ_x - boundary layer displacement thickness

ε - crossflow angle

ν - kinematic viscosity

ϕ - pitch angle

θ - yaw angle

θ_{cal} - yaw angle for nulling five-hole probe during calibration

θ_{meas} - uncorrected yaw angle

θ_x - boundary layer momentum thickness

Subscripts

ms - main flow

w - wall

1,2 = indices

References

1. Nash, J. F. and Patel, V. C., Three-Dimensional Turbulent Boundary Layers, SBC Technical Books, Atlanta, 1972.

2. Maskell, E. C., "Flow Separation in Three Dimensions", Report No. Aero 2565, Royal Aircraft Establishment, Farnborough, November 1955.

3. Taylor, E. S., "Some Problems of Recognizing and Defining Separation of the Skewed Boundary Layer", Fluid Mechanics of Internal Flow, Edited by G. Sovran, Elsevier, Amsterdam, 1967, pp.320-332.

4. Lighthill, M. J., Laminar Boundary Layers, Edited by L. Rosenhead, Oxford University Press, pp.60-82.

5. Oswatitsch, K.,"Die Ablosungsbedingung von Grenzschichten", Symposium on Boundary Layer Research, International Union of Theoretical and Applied Mechanics, Edited by Gortler, Springer Verlay, Berlin, 1958.

6. Krcnauer, R. E., Fluid Mechanics of Internal Flow, Edited by G. Sovran, Elsevier, Amsterdam, 1967, p.331

7. Perry, A. E. and Fairlie, B. D., "Critical Points in Flow Patterns", Advanced Geophysics, vol. B18, pp.299-315.

8. Smith, P. D., A note on the computation of the inviscid rotational flow past the trailing edge of an aerofoil, R.A.E. Tech. Memo Aero 1217, 1970.

9. Fairlie, B. D., "A Study of Separation in Turbulent Boundary Layers", Ph.D. Thesis, University of Melbourne, Melbourne.

10. Hunt, J.C.R., Abell, C. J., Peterka, J. A., and Woo, H., "Kinematical Studies of the Flows Around Free or Surface-Mounted Obstacles; Applying Topology to Flow Visualization", Journal of Fluid Mechanics, vol. 86, pp.179-201.

11. Flegg, G. C., From Geometry to Topology, English Universities Press, 1974.

12. Prandtl, L., "Uber Reibungsschlichten bei dreidimensionalen Stromungen", British M.A.P. Volkenrode Rep. and Trans. No.64, 1946.

13. Mager, A., "Generalization of Boundary Layer Momentum Integral Equations to Three Dimensional Flows Including Those of Rotating Systems", NACA Report No. 1067, 1952.

14. Moore, Jr., R. W. and Richardson, D. L., "Skewed Boundary Layers Near the End Walls of a Compressor Cascade", Trans. ASME, vol. 79, 1957, pp.1789-1800.

15. von Doenhoff, A. E. and Tetervin, N., "Determination of General Relations for the Behavior of Turbulent Boundary Layers", NACA Report No. 772, 1943.

16. Squire, H. B. and Winter, K. G., "The Secondary Flow in a Cascade of Airfoils in a Non-uniform Stream", Journal of the Aeronautical Sciences, vol. 18, 1951, pp.271-277.

17. Taylor, E. S., "The Skewed Boundary Layer", Trans. ASME, Series D, Journal of Basic Engineering, vol. 18, 1959, pp.297-304.

18. Johnston, J. P., "On the Three-Dimensional Boundary Layer Generated by Secondary Flow", Trans. ASME, Journal of Basic Engineering, vol. 82, 1960, pp.233-248.

19. Clauser, F. H., "Turbulent Boundary Layers in Adverse Pressure Gradients", Journal of the Aeronautical Sciences, vol. 21, 1954, pp.91-108.

20. Ludweig, H. and Tillman, W., "Investigation of the Wall Shearing Stress in Turbulent Boundary Layers", NACA TM 1285, May 1952.

21. Eichenberger, H. P., Comments in Trans. ASME, Journal of Basic Engineering, vol. 81, 1959, pp.301-302.

22. Hawthorne, W. R., "Engineering Abstracts", Research Frontiers in Fluid Dynamics, edited by R. J. Seeger and G. Temple, John Wiley and Sons, 1965, pp.1-29.

23. Townsend, A. A., The Structure of Turbulent Shear Flow, Cambridge University Press, 1956, p.232.

24. Johnston, J. P., "The Turbulent Boundary Layer at a Plane of Symmetry in a Three-Dimensional Flow", Trans. ASME, Journal of Basic Engineering, vol. 82, 1960, pp.622-628.

25. Hornung, H. G. and Joubert, P. N., "The Mean Velocity Profile in Three-Dimensional Turbulent Boundary Layers", Journal of Fluid Mechanics, vol. 15, 1963, pp.368-384.

26. Kliensiek, W. F. and Pierce, F. J., "Simultaneous Lateral Skewing in a Three-Dimensional Turbulent Layer Flow", Trans. ASME, Journal of Basic Engineering, vol. 92, 1970, pp.83-92.

27. Langston, L. S., "Crossflows in a Turbine Cascade Passage", Trans. ASME, Journal of Engineering for Power, vol. 102, October, 1980, pp.866-874.

28. Eichelbrenner, E. A., "Theoretical Investigation and Control by Measuring Tests on the Behavior of the Three-Dimensional Turbulent Boundary Layer on an Annular Wing at Various Incidences", Bureau Technique Zborowski, Brunoy, 1963.

29. Johnston, J. P., "Experimental Studies in Three-Dimensional Turbulent Boundary Layers", Report MD-34, Dept. of Mech. Engineering, Stanford University, July 1976.

30. Wheeler, A. J. and Johnston, J. P., "An Assessment of Three-Dimensional Turbulent Boundary Layer Prediction Methods", ASME Journal of Fluids Engineering, September 1973, pp.415-421.

31. Pratap, V. S. and Spalding, D. B., "Fluid Flow and Heat Transfer in Three-Dimensional Duct Flows", Int. Journal of Heat and Mass Transfer, vol. 19, 1976, pp.1183-1188.

32. Briley, W. R. and MacDonald, H., "Computation of Three-Dimensional Subsonic Flow in Curved Passages", United Aircraft Research Laboratory Report R75-911596-8, 1975.

33. Dodge, P. R., "A Numerical Method for Two and Three-Dimensional Viscous Flows", AIAA Paper No. 76-425, AIAA 9th Plasma and Fluid Dynamics Conf., San Diego, CA 1976.

34. Ghia, K. N., Ghia, V., and Studerus, C. J., "Analytical Formulation of Three-Dimensional Laminar Viscous Flow through Turbine Cascades Using Surface Oriented Coordinates", ASME Paper No. 76-EE-22, 1976.

35. Briley, W. R. and MacDonald, H., "Computation of Three-Dimensional Horseshoe Vortex Flow Using the Navier Stokes Equations", Proc. 7th Int. Conf. on Num. Methods in Fluid Dyn., Stamford, 1980.

36. Briley, W. R. and MacDonald, H., "Computation of Turbulent Horseshoe Vortex Flow Past Swept and Unswept Leading Edges", Final Report for contract N000 14-77-C-007S to the Office of Naval Research, March 1982.

37. Shabaka, I.M.M.A., "Turbulent Flow in an Idealized Wing-Body Junction", Ph.D. Thesis, Imperial College of Science and Technology, London, England, April 1979.

38. Langston, L. S., Nice, M. L. and Hooper, R. M., "Three-Dimensional Flow Within a Turbine Cascade Passage", Trans. ASME, Journal of Engineering for Power, vol. 99, January 1977, pp.21-28.

39. Ram, V. V., "Untersuchungen uber die Eckengrenzschicht an einem Kreiszylinder mit Seitenwand", Report 63/46, Institute of Fluid Mechanics, Technische Hochschule, Braunschweig, 1963.

40. Belik, L., "The Secondary Flow about Circular Cylinders Mounted Normal to a Flat Plate", Aeronautical Quarterly, February 1973, pp.47-54.

41. East, L. F. and Hoxey, R. P., "Low Speed Three-Dimensional Turbulent Boundary Layer Data", Royal Aircraft Establishment, Tech. Rep. No. 69041, Parts I and II, 1969.

42. Baker, C. J., "Vortex Flow Around the Bases of Obstacles", Ph.D. Thesis, University of Cambridge, Cambridge, England, September 1978.

43. Peake, D. J. and Galway, R. D., "The Three-Dimensional Separation of a Plane Incompressible Laminar Boundary Layer Produced by a Circular Cylinder Mounted Normal to a Flat Plate", Developments in Boundary Layer Research, Agardograph 97, Part II, May 1965, pp.1049-1080.

44. Taniguchi, S., Hiroshi, S. and Arie, M., "Flow Around a Cylinder Mounted in a Turbulent Boundary Layer", Bul. of the JSME, vol. 24, No. 193, July 1981, pp.1130-1136.

45. Mojola, O. O., "Measurements in a Turbulent Horseshoe Vortex and the Problem of Probe Interference", Imperial College of Science and Technology Report I.C. Aero Report 73-08, December 1973.

46. Langston, L. S., "Turbine Endwall Two-Cylinder Program", Semi-Annual Status Report, January 1, 1979 - July 1, 1979.

47. Ibid., July 1, 1979 - January 1, 1980.

48. Ibid., January 1, 1980 - July 1, 1980.

49. Ibid., July 1, 1980 - January 1, 1981.

50. Ibid., January 1, 1981 - July 1, 1981.

51. Camarata, F. J., Hooper, R. M. and Nice, M. C., "Experimental Investigation of Passage Flow in Baseline Build of Large-Scale Turbine Cascade", United Aircraft Research Labs Report R75-212632, June 1975.